

# Emergence of curved momentum-spacetime and its effect on the cyclotron motion in the antiferromagnetic quantum critical metal

Francisco Borges<sup>1,2a</sup> and Sung-Sik Lee<sup>1,2b</sup>

<sup>1</sup>*Department of Physics & Astronomy, McMaster University, Hamilton ON L8S 4M1, Canada*

<sup>2</sup>*Perimeter Institute for Theoretical Physics, Waterloo ON N2L 2Y5, Canada*

(Dated: May 5, 2023)

We show that anisotropic quantum corrections can dynamically give rise to curved momentum-spacetimes for quasiparticles in metals. In the (2+1)-dimensional antiferromagnetic quantum critical metal, a curved momentum-spacetime arises as the critical spin fluctuations generate red shift that dilates frequency of electron unevenly on the Fermi surface. As the disparity of the momentum-dependent red shift is controlled by the shape of the Fermi surface, the momentum-spacetime geometry that emerges at low energies depends on the bare nesting angle of the Fermi surface. With increasing nesting angle, the region in which electron motion is slowed down by critical spin fluctuations shrinks. On the other hand, the increasing nesting angle makes the red shift stronger near the hot spots due to the weakened screening of the interaction. These competing effects result in a non-monotonic dependence of the cyclotron frequency of electron on the nesting angle of the Fermi surface. The red shift that becomes more singular at the hot spots with increasing nesting angle creates a possibility of realizing a momentum-space black hole horizon beyond a critical nesting angle : the electron motion becomes ‘perpetually’ slowed down as it approaches a hot spot in the same way that the motion of a free falling object freezes near the event horizon of a black hole with respect to an asymptotic observer. However, the analogous horizon in momentum space does not lead to a vanishing cyclotron frequency because the metric singularity at the hot spots is cut off by thermal effects present above the non-zero superconducting transition temperature.

## I. Introduction

The semi-classical equation of motion of quasiparticles in solids is remarkably symmetric under the interchange of position and momentum. The momentum-dependent quasiparticle energy is the counter part of the position-dependent potential in real space. The Berry curvature associated with the Bloch wavefunctions plays the role of the magnetic field in momentum space[1]. It is then natural to ask if the symmetry can be further extended to spacetime geometry[2–6]. A real-space curvature can be created through buckling of lattices or topological defects in solids[7–12]. Recently, it has been pointed out that the non-linear response of quasiparticles to the external electromagnetic field can be captured through the geodesic equation in a curved momentum-space[13]. In this paper, we consider an intrinsic physical mechanism by which momentum space and time is integrated into a curved *momentum-spacetime*. We point out that curved momentum-spacetimes naturally arise from anisotropic quantum corrections in metals and even a momentum-space black hole horizon can emerge if quantum corrections are strongly singular in momentum space.

Strongly momentum-dependent quantum corrections arise in metals close to quantum critical points associated with order parameters carrying non-zero momenta. At spin or charge density-wave critical points, electrons residing on hot manifolds, sub-manifolds of Fermi surface that can be connected by the ordering wavevectors, are more strongly scattered by critical fluctuations than electrons away from the hot manifolds. This leads to a momentum-dependent renormalization of electron. In particular, the Fermi velocity can acquire a strong dependence on momentum along the Fermi surface as electrons become significantly heavier near the hot manifold. Interestingly, a strongly momentum-dependent Fermi velocity can arise as a consequence of momentum-dependent red shift even without a direct renormalization of the band dispersion energy. Namely, the Fermi velocity can acquire momentum-dependence through a momentum-dependent dilatation of frequency : a quantum correction to the frequency-dependent kinetic term of electron is translated into a renormalization of the Fermi velocity. This momentum-dependent red shift is indeed the primary mechanism by which the Fermi velocity acquires a strong momentum dependence in the antiferromagnetic quantum critical metal in two space dimensions[14]. In such cases, one can understand phenomena associated with momentum-dependent Fermi velocity as consequences of a curved momentum-spacetime geometry. The same physics can be understood without invoking a curved momentum-spacetime<sup>1</sup>. However, such non-geometric descriptions require introducing features that are rather arbitrary and finely tuned. For example, through the momentum-dependent

<sup>a</sup> fborges@perimeterinstitute.ca

<sup>b</sup> slee@mcmaster.ca

<sup>1</sup> Just as the effects of curved spacetime in general relativity can be still described within the Newtonian framework.

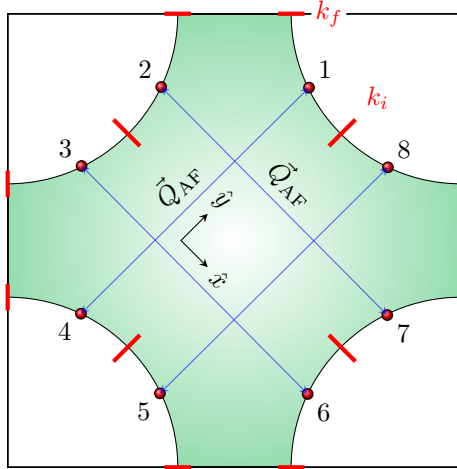


**FIG. 1:** The full Fermi surface divided into eight segments. Segment 1 is bounded by  $k_i$  and  $k_f$ , and other segments are related to it through the  $C_4$  and reflection symmetries. Each segment contains one hot spot denoted as red dots on the Fermi surface. The hot spots are connected by the antiferromagnetic ordering wave vector,  $\vec{Q}_{AF}$ .  $\hat{x}$  ( $\hat{y}$ ) is chosen to be perpendicular (parallel) to  $\vec{Q}_{AF}$  at hot spot 1.

red shift, only the magnitude of the Fermi velocity is renormalized even if the direction is not protected by generic quantum corrections that renormalize the Fermi velocity. In the geometric description, it is naturally captured as a renormalization of the temporal metric. For this reason, we adopt the geometric perspective to describe the dynamics of quasiparticles that are subject to momentum-dependent quantum corrections.

The antiferromagnetic quantum criticality is believed to play an important role in electron doped cuprates[15], iron pnictides[16], and heavy fermion compounds[17]. Although the theory in two space dimensions becomes strongly interacting at low energies, it is solvable in the limit that the bare nesting angle is small[14, 18]. While electrons at the hot spots remain coupled with critical spin fluctuations down to the zero energy limit[19–40], electrons away from the hot spots are decoupled from spin fluctuations at sufficiently low energies. Since the crossover energy scale for the decoupling depends on momentum relative to the hot spots, quasiparticles are renormalized with a momentum-dependent red shift, which gives rise to a curved momentum-spacetime. If the momentum-dependent metric is singular enough, the emergent geometry can exhibit an analogous black hole horizon whose presence affects the dynamics of quasiparticles significantly. For example, the curved momentum-spacetime geometry directly manifests itself in the cyclotron motion of quasiparticles[41–51].

Here is the outline of the paper. In Sec. **II**, we start by reviewing the field-theoretical functional renormalization group study of the antiferromagnetic quantum critical metal[14] with an emphasis on the results that are needed for the present work. We then cast the theory of the fully renormalized quasiparticles away from the hot spots into a theory of spinor propagating in a curved momentum-spacetime. In Sec. **III**, we compute the cyclotron period of electron as a function of the bare nesting angle of the Fermi surface. We show that the unusual dependence of the cyclotron period on the nesting angle is a result of the non-trivial evolution of the curved momentum-spacetime geometry with varying nesting angle. We conclude with a summary in Sec. **IV**.

## II. Emergence of a curved momentum-spacetime

In this section, we first review the theory of the antiferromagnetic quantum critical metal in  $2 + 1$  dimensions, focusing on the renormalized shape of the Fermi surface and the Fermi velocity that control the dynamics of low-energy quasiparticles. In order to capture the momentum profiles of the coupling functions across the Fermi surface,

we need to consider the low-energy effective field theory that includes all gapless modes on the Fermi surface[14],

$$\begin{aligned}
S = & \sum_{N=1}^8 \sum_{\sigma=1}^{N_c} \sum_{j=1}^{N_f} \int d\mathbf{k} \psi_{N,\sigma,j}^\dagger(\mathbf{k}) \left\{ ik_0 + V_{F,k_N}^{(N)} e_N[\vec{k}; v_{k_N}^{(N)}] \right\} \psi_{N,\sigma,j}(\mathbf{k}) \\
& + \frac{1}{\sqrt{N_f}} \sum_{N=1}^8 \sum_{\sigma\sigma'=1}^{N_c} \sum_{j=1}^{N_f} \int d\mathbf{k} d\mathbf{q} g_{k_N+q_N, k_N}^{(N)} \psi_{N,\sigma',j}^\dagger(\mathbf{k} + \mathbf{q}) \Phi_{\sigma'\sigma}(\mathbf{q}) \psi_{N,\sigma,j}(\mathbf{k}) \\
& + \frac{1}{4\mu} \sum_{\{N_i=1\}}^8 \sum_{\{\sigma_i=1\}}^{N_c} \sum_{\{j_i=1\}}^{N_f} \int \prod_{i=1}^4 d\mathbf{k}_i \delta_{1+2,3+4} \lambda_{\left(\begin{array}{cc} N_1 & N_2 \\ N_4 & N_3 \\ k_1; N_1 & k_2; N_2 \\ k_4; N_4 & k_3; N_3 \end{array}\right); \left(\begin{array}{cc} \sigma_1 & \sigma_2 \\ \sigma_4 & \sigma_3 \end{array}\right)} \psi_{N_1,\sigma_1,j_1}^\dagger(\mathbf{k}_1) \psi_{N_2,\sigma_2,j_2}^\dagger(\mathbf{k}_2) \psi_{N_3,\sigma_3,j_3}(\mathbf{k}_3) \psi_{N_4,\sigma_4,j_4}(\mathbf{k}_4).
\end{aligned} \tag{1}$$

Here, we consider a Fermi surface with the  $C_4$  and reflection symmetries that supports eight hot spots labelled by  $N = 1, 2, \dots, 8$  as is shown in Fig. 1. The Fermi surface is divided into eight disjoint segments whose union covers the entire Fermi surface. Each segment, which contains one hot spot, is labelled by the associated hot spot index.  $\psi_{N,\sigma,j}(\mathbf{k})$  represents the electron field in segment  $N$  with spin  $\sigma = 1, 2, \dots, N_c$  and flavour  $j = 1, 2, \dots, N_f$ . The electron is in the fundamental representations of spin  $SU(N_c)$  and flavour  $SU(N_f)$  groups. The case that is most relevant to experiments is  $N_c = 2$  and  $N_f = 1$ , but we keep  $N_c$  and  $N_f$  general because the solution obtained in the small nesting angle limit is valid for any  $N_c \geq 2$  and  $N_f \geq 1$ .  $d\mathbf{k} \equiv \frac{dk_0 dk_x dk_y}{(2\pi)^3}$ , where  $\mathbf{k} = (k_0, \vec{k}) = (k_0, k_x, k_y)$  denotes three-vector that includes the Matsubara frequency  $k_0$  and the two-dimensional momentum  $\vec{k}$  which is measured relative to the hot spot in each segment. The collective antiferromagnetic spin fluctuations are represented by a bosonic field  $\Phi(\mathbf{q}) = \sum_{a=1}^{N_c^2-1} \phi^a(\mathbf{q}) \tau^a$ , where  $\tau^a$ 's denote the  $N_c \times N_c$  generators of  $SU(N_c)$  with  $\text{Tr}[\tau^a \tau^b] = 2\delta_{ab}$  and  $\vec{q}$  is measured relative to the ordering wavevector,  $\vec{Q}_{AF}$ . We consider the case where  $2\vec{Q}_{AF}$  is equivalent to a reciprocal vector and  $\phi^a(\mathbf{q}) = \phi^a(-\mathbf{q})^*$ . The momentum conserving delta function is denoted as  $\delta_{1+2,3+4} \equiv (2\pi)^3 \delta(\mathbf{k}_1 + \mathbf{k}_2 - \mathbf{k}_3 - \mathbf{k}_4)$ .  $k_N$  represents the component of momentum that labels the Fermi surface in segment  $N$ ,

$$k_N = \begin{cases} k_x & \text{for } N = 1, 4, 5, 8 \\ k_y & \text{for } N = 2, 3, 6, 7 \end{cases}.$$

Although neither  $\hat{x}$  nor  $\hat{y}$  direction is perfectly parallel to the Fermi surface in general, there is one-to-one correspondence between  $k_N$  and a point on the Fermi surface in each segment.  $V_{F,k_N}^{(N)}$  is the momentum-dependent Fermi velocity in the direction parallel to  $\vec{Q}_{AF}$  in segment  $N$ .  $e_N[\vec{k}; v_{k_N}^{(N)}]$  specifies the Fermi surface in segment  $N$  through

$$\begin{aligned}
e_1[\vec{k}; v_{k_x}^{(1)}] &= v_{k_x}^{(1)} k_x + k_y, & e_2[\vec{k}; v_{k_y}^{(2)}] &= -v_{k_y}^{(2)} k_y - k_x, & e_3[\vec{k}; v_{k_y}^{(3)}] &= v_{k_y}^{(3)} k_y - k_x, & e_4[\vec{k}; v_{k_x}^{(4)}] &= v_{k_x}^{(4)} k_x - k_y, \\
e_5[\vec{k}; v_{k_x}^{(5)}] &= -v_{k_x}^{(5)} k_x - k_y, & e_6[\vec{k}; v_{k_y}^{(6)}] &= v_{k_y}^{(6)} k_y + k_x, & e_7[\vec{k}; v_{k_y}^{(7)}] &= -v_{k_y}^{(7)} k_y + k_x, & e_8[\vec{k}; v_{k_x}^{(8)}] &= -v_{k_x}^{(8)} k_x + k_y.
\end{aligned} \tag{2}$$

If  $v_k^{(N)} = 0$ , pairs of segments connected by  $\vec{Q}_{AF}$  become perfectly nested. In general,  $v_k^{(N)}$  is non-zero and  $k$ -dependent. For this reason, we call  $v_k^{(N)}$  momentum-dependent nesting angle. The Yukawa coupling denoted as  $g_{k',k}^{(N)}$  is a function of initial and final momenta of electrons. Similarly,  $\lambda_{\left(\begin{array}{cc} N_1 & N_2 \\ N_4 & N_3 \\ k_1 & k_2 \\ k_4 & k_3 \end{array}\right); \left(\begin{array}{cc} \sigma_1 & \sigma_2 \\ \sigma_4 & \sigma_3 \end{array}\right)}$  denotes the short-range four-fermion interaction labeled by momenta of electrons on the Fermi surface. The coupling functions in different segments are related to each other through symmetry, and  $v_k^{(N)}$ ,  $V_{F,k}^{(N)}$  and  $g_{k',k}^{(N)}$  can be written as

$$\left( v_k^{(N)}, V_{F,k}^{(N)}, g_{k',k}^{(N)} \right) = \begin{cases} (v_k, V_{F,k}, g_{k',k}), & N = 1, 3, 4, 6 \\ (v_{-k}, V_{F,-k}, g_{-k',-k}), & N = 2, 5, 7, 8 \end{cases}. \tag{3}$$

Similarly, four-fermion coupling functions that are mapped to each other under the symmetry are related.

In Eq. (1),  $\mu$  is the floating energy scale at which the vertex functions that depend on momenta along the Fermi surface are identified with the coupling functions. For example, the momentum-dependent nesting angle and Fermi velocity at scale  $\mu$  are defined through

$$Re\Gamma_1^{(2,0)}(\mathbf{k}) \Big|_{\mathbf{k}=(\mu, k_x, -v_{k_x} k_x)} = 0, \quad \frac{\partial}{\partial k_y} Re\Gamma_1^{(2,0)}(\mathbf{k}) \Big|_{\mathbf{k}=(\mu, k_x, -v_{k_x} k_x)} = V_{F,k_x}, \tag{4}$$

where  $\Gamma_1^{(2,0)}(\mathbf{k})$  is the two-point vertex function of electron in segment 1 and the field is normalized so that  $\frac{\partial}{\partial k_0} Im\Gamma_1^{(2,0)}(\mathbf{k}) \Big|_{\mathbf{k}=(\mu, k_x, -v_{k_x} k_x)} = i$ . The power of  $\mu$  in front of each coupling function denotes its scaling dimension under the interaction driven scaling[52] that is exact in the limit that the nesting angle is small[18]. The

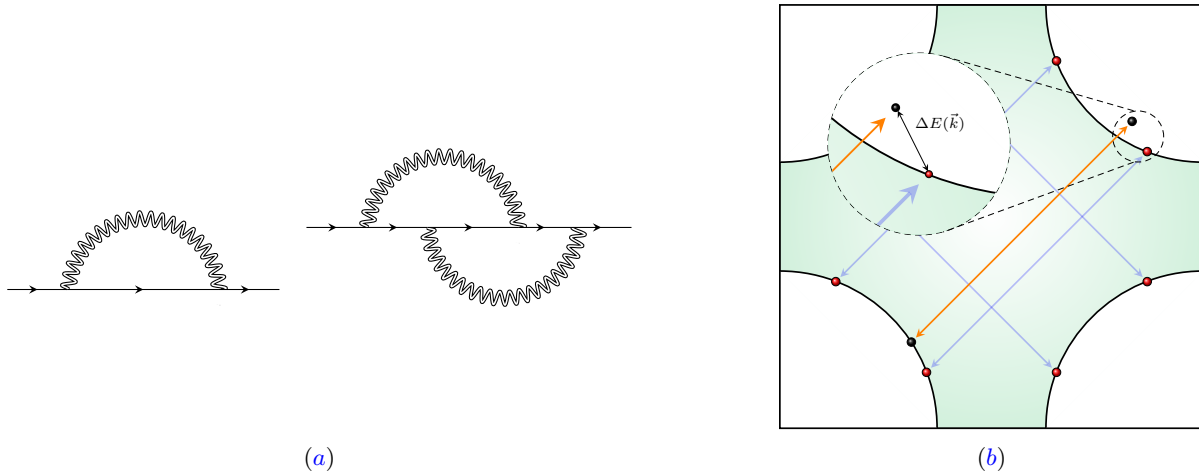


**FIG. 2:** (a) The leading quantum corrections that dress the quadratic action of electron in the limit that the nesting angle is small. The double wiggly line represents the fully dressed boson propagator obtained from the Schwinger-Dyson equation[18]. (b) The virtual electron created when an electron near hot spot 5 emits a boson with zero energy. If the electron is right at the hot spot 5, it is scattered onto the hot spot 8 on the Fermi surface. If the electron is away from the hot spot, it is scattered into a state away from the Fermi surface. The non-zero energy of the virtual particle ( $\Delta E(\vec{k})$ ) cuts off the IR singularity of the self-energy.

four-fermion coupling function, which has scaling dimension  $-1$ , should be included in the renormalizable theory because it is promoted to a marginal coupling with the help of the Fermi momentum[14]. On the contrary, quartic boson couplings are strictly irrelevant under the interaction-driven scaling and can be dropped in the low-energy theory[18]. The low-energy theory does not include the quadratic action of the boson either because the local kinetic term is irrelevant under the interaction driven scaling<sup>2</sup>. The absence of the bare boson kinetic term in the action gives us the freedom to rescale the boson field to tune the magnitude of the Yukawa coupling at the hot spots. The physics does not depend on this choice, but it is convenient to choose the normalization so that  $g_{0,0} = \sqrt{\pi v_0/2}$ . With this

choice, the boson self-energy is ‘canonically’ normalized to  $D(\mathbf{q})^{-1} = |q_0| + c(|q_x| + |q_y|)$ , where  $c = \sqrt{\frac{v_0}{8N_c N_f} \log\left(\frac{1}{v_0}\right)}$  is the speed of the dressed collective mode that is entirely determined from the nesting angle at the hot spots[18]. We also have the freedom to choose the scale of frequency relative to momentum. We first follow Ref. [14] to choose the unit of frequency such that  $V_{F,0} = 1$  at all scales<sup>3</sup>. Since the electrons at the hot spots receive quantum corrections down to the zero energy limit, keeping  $V_{F,k} = 1$  in Eq. (4) at all  $\mu$  requires a continuous redefinition of  $k_0$  relative to the bare frequency as the energy scale is lowered. Since we are using one global clock according to which the electrons at the hot spots have a fixed velocity, cold electrons away from the hot spots appear to be moving faster with this choice of frequency unit.

The evolution of the momentum-dependent vertex function with decreasing  $\mu$  defines the functional renormalization group flow of the coupling functions[14]. In the space of coupling functions, an *interacting* fixed point arises at

$$v_k = 0, \quad V_{F,k} = 1, \quad g_{k',k} = 0, \quad \lambda \begin{pmatrix} N_1 & N_2 \\ N_4 & N_3 \\ k_1 & k_2 \\ k_1 + k_2 - k_3 & k_3 \end{pmatrix} = 0 \quad (5)$$

with  $g_{k',k}^2/v_k = \pi/2$ . Although the couplings vanish at the fixed point, quantum corrections remain non-trivial due to the vanishing nesting angle at the fixed point. The anomalous dimension of the boson is controlled by  $g_{k',k}^2/v_k \sim O(1)$  and Eq. (5) is far from the Gaussian fixed point. For theories with non-zero nesting angles at UV, the coupling functions undergo a non-trivial renormalization group flow as energy is lowered. At low energies, the coupling functions acquire momentum dependence under the functional renormalization group flow because quantum corrections depend on momentum along the Fermi surface. In this paper, we consider the case, where  $v_k$  and  $V_{F,k}$  are independent of momentum at UV cutoff scale  $\Lambda$ :  $v_k(\ell = 0) = v_0(0)$  and  $V_{F,k}(\ell = 0) = 1$ , where  $\ell \equiv \log \Lambda/\mu$  is

<sup>2</sup> Physically, this implies that the two-point function of the boson is entirely determined by quantum corrections at low energies.

<sup>3</sup> With this choice,  $V_{F,k}$  at  $k \neq 0$  represents the Fermi velocity measured in the unit of the Fermi velocity at the hot spots.

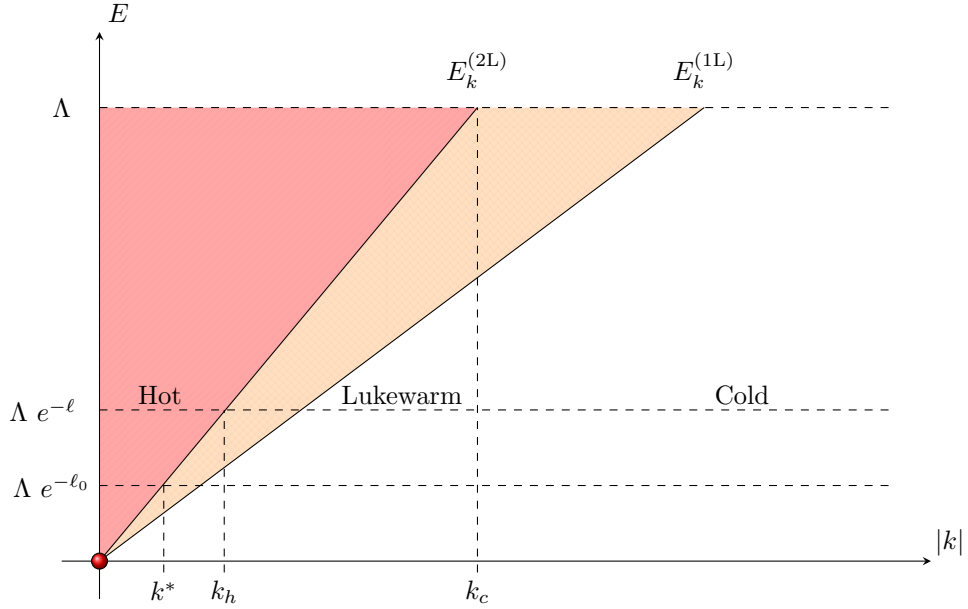


**FIG. 3:** Crossover energy scales associated with the two-loop fermion self-energy ( $E_k^{(2L)}$ ) and one-loop fermion and the one-loop fermion self-energy ( $E_k^{(1L)}$ ), respectively. At a small nesting angle, the flow of couplings between the two crossover energy scales is negligible, and one can use the approximation in which both quantum corrections turn off simultaneously below  $E_k^{(2L)}$ . At energy scales  $\mu = \Lambda e^{-\ell}$ , the momentum space is divided into three regions depending on the magnitude of  $E_k^{(2L)}$  relative to  $\mu$  and  $\Lambda$ .  $\mu_0 \equiv \Lambda e^{-\ell_0}$  denotes the energy scale below which the flow of the nesting angle becomes important. In  $k < k^*$ , the shape of the Fermi surface is significantly renormalized.

the logarithmic length scale. For different UV theories, the exact profiles of the renormalized coupling functions are different, but the part that is singular at the hot spots is universal[14].

In the small nesting angle limit, only the one-loop and two-loop fermion self-energy corrections are important for the quadratic action of electrons (Fig. 2(a)). If the external electron is right at a hot spot, the electron can be scattered to another hot spot by emitting virtual bosons with zero energy. Since all virtual particles can have zero energy in the loop, a logarithmic singularity arises for electrons at hot spots. If the external electron is away from hot spots, virtual particles are forced to carry a non-zero energy. The energy, which is proportional to the deviation of momentum away from the hot spot and the nesting angle, cuts off the infrared singularity as is illustrated in Fig. 2(b). Because of this, electrons away from hot spots become decoupled from spin fluctuations at sufficiently low energies. The crossover energy scales for the one-loop and two-loop fermion self-energy of the electron on the Fermi surface with momentum  $k = k_N$  relative to the hot spots are given by

$$E^{(1L)} = 2cv_k |k|, \quad E^{(2L)} = 4V_{F,k}v_k |k|. \quad (6)$$

These crossover energy scales as functions of  $k$  are shown in Fig. 3. Each quantum correction turns off at energies far below  $E_k^{(1L)}$  and  $E_k^{(2L)}$ , respectively. For later uses, we write the logarithmic length scales associated with Eq. (6) as

$$\ell_k^{(1L)} = \log\left(\frac{\Lambda}{2cv_k|k|}\right), \quad \ell_k^{(2L)} = \log\left(\frac{\Lambda}{4V_{F,k}v_k|k|}\right). \quad (7)$$

At a given logarithmic length scale  $\ell$ , there exist two momentum scales  $k_c$  and  $k_h$  that divide the momentum space into three regions. In the ‘cold’ region with  $k > k_c$ , electrons are too far away from the hot spots to receive a significant quantum correction at energies below  $\Lambda$ . In the ‘lukewarm’ region with  $k_h < k < k_c$ , electrons receive non-trivial quantum corrections at energies below  $\Lambda$  but becomes largely decoupled from spin fluctuations at scale  $\ell$ . In the ‘hot’ region with  $k < k_h$ , electrons remain strongly coupled with critical spin fluctuations at scale  $\ell$ .  $k_c$  and  $k_h$

are determined from the conditions,  $\ell_{k_c}^{(2L)} = 0$  and  $\ell_{k_h}^{(2L)} = \ell$ , respectively<sup>4</sup>. Electrons at different points on the Fermi surface are decoupled from spin fluctuations at different energy scales. As a result, the coupling functions at different locations on the Fermi surface receive quantum corrections for different durations of RG ‘time’ as the energy scale is lowered from  $\Lambda$  to 0. This results in non-trivial momentum profiles of the coupling functions at low energies.

At a low energy scale with a large but finite  $\ell$ , the quadratic theory is written as

$$S_{\text{kin}} = \sum_{N=1}^8 \sum_{\sigma=1}^{N_c} \sum_{j=1}^{N_f} \int d\mathbf{k} \psi_{N,\sigma,j}^\dagger(\mathbf{k}) \left\{ ik_0 + V_{F,k_N}^{(N)} e_N \left[ \vec{k}; v_{k_N}^{(N)} \right] \right\} \psi_{N,\sigma,j}(\mathbf{k}), \quad (8)$$

where the renormalized nesting angle  $v_k$  and Fermi velocity  $V_{F,k}$  have the profiles[14],

$$v_k = \begin{cases} v_0(\ell) & 0 \leq k < k_h \\ v_0(\ell_k^{(2L)}) & k_h \leq k < k_c \\ v_0(0) & k_c \leq k \end{cases}, \quad V_{F,k} = \begin{cases} 1 & 0 \leq k < k_h \\ \mathcal{E}_1(\ell; \ell_k^{(2L)}) & k_h \leq k < k_c \\ \mathcal{E}_1(\ell; 0) & k_c \leq k \end{cases}. \quad (9)$$

Here,  $v_0(X) = \frac{\pi^2 N_c N_f}{2(N_c^2 - 1)} \frac{1}{(X + \ell_0) \log(X + \ell_0)}$ ,  $\mathcal{E}_1(X, Y) = \exp \left( \sqrt{N_c^2 - 1} \left( \text{Ei}(\log \sqrt{X + \ell_0}) - \text{Ei}(\log \sqrt{Y + \ell_0}) \right) \right)$  with  $\text{Ei}(x)$  being the exponential integral function and

$$\ell_0 = \frac{\pi^2 N_c N_f}{2(N_c^2 - 1)} \frac{1}{v_0(0) \log(1/v_0(0))} \quad (10)$$

represents the logarithmic length scale below which the flow of the nesting angle is negligible.

In the strict zero temperature limit, the theory develops superconducting instabilities due to the run-away flow of the four-fermion coupling function[14]. However, the normal state remains stable down to an energy scale that is exponentially small in  $1/\sqrt{v_0(0)}$  in the limit that  $v_0(0)$  is small and the bare four-fermion coupling is weak. Here, we study the dynamics of electrons at energies low enough that electrons are decoupled from the critical spin fluctuations almost everywhere on the Fermi surface except for the immediate vicinity of the hot spots but high enough that the superconducting instability is absent. As a first step, we consider the dynamics of quasiparticles at zero temperature, ignoring the superconducting instability. Later, we consider the thermal effect that arises above the superconducting transition temperature.

At zero energy ( $\ell = \infty$ ), the Fermi velocity in Eq. (9) becomes infinite away from the hot spot. This is because we are using the rescaled clock with respect to which the speed of electrons at the hot spots, which is infinitely slower than cold electrons, is 1. While this clock is convenient for describing the scaling behaviour of electrons at the hot spots and the critical spin fluctuations[18], it is not useful for describing the dynamics of electrons away from the hot spots. For electrons away from hot spots, it is more convenient to use the bare clock with respect to which the velocity of the cold electrons is fixed to be 1. We can go back to the bare unit of frequency by undoing the rescaling the frequency as

$$k_0 = \left( \frac{V_{F,k_c}^{(N)}}{V_{F,0}^{(N)}} \right) \omega, \quad \psi_{N,\sigma,j}(\mathbf{k}) = \left( \frac{V_{F,k_c}^{(N)}}{V_{F,0}^{(N)}} \right)^{-1} \tilde{\psi}_{N,\sigma,j}(\omega, \vec{k}), \quad (11)$$

where the normalization of the field is chosen to keep the canonical form of the action,

$$S_{\text{kin}} = \sum_{N=1}^8 \sum_{\sigma=1}^{N_c} \sum_{j=1}^{N_f} \int \frac{d\omega d^2 \vec{k}}{(2\pi)^3} \tilde{\psi}_{N,\sigma,j}^\dagger(\omega, \vec{k}) \left\{ i\omega + \mathcal{V}_{F,k_N}^{(N)} e_N \left[ \vec{k}; v_{k_N}^{(N)} \right] \right\} \tilde{\psi}_{N,\sigma,j}(\omega, \vec{k}). \quad (12)$$

Here,  $\mathcal{V}_{F,k_N}^{(N)} = \left( \frac{V_{F,0}^{(N)}}{V_{F,k_c}^{(N)}} \right) V_{F,k_N}^{(N)}$  denotes the Fermi velocity measured in the bare time. In the low-energy limit,  $k_h$  approaches zero and the hot region shrinks to points. This implies that quasiparticles are well defined everywhere on

<sup>4</sup> Strictly speaking, one has to use  $\ell_{k_c}^{(1L)} = 0$  and  $\ell_{k_h}^{(1L)} = \ell$  to determine  $k_c$  and  $k_h$  because because  $E_k^{(1L)} < E_k^{(2L)}$ . However, we can use either  $E_k^{(1L)}$  or  $E_k^{(2L)}$  in the limit that the nesting angle is small because the differences of the couplings at  $E_k^{(1L)}$  and  $E_k^{(2L)}$  are negligible[14].

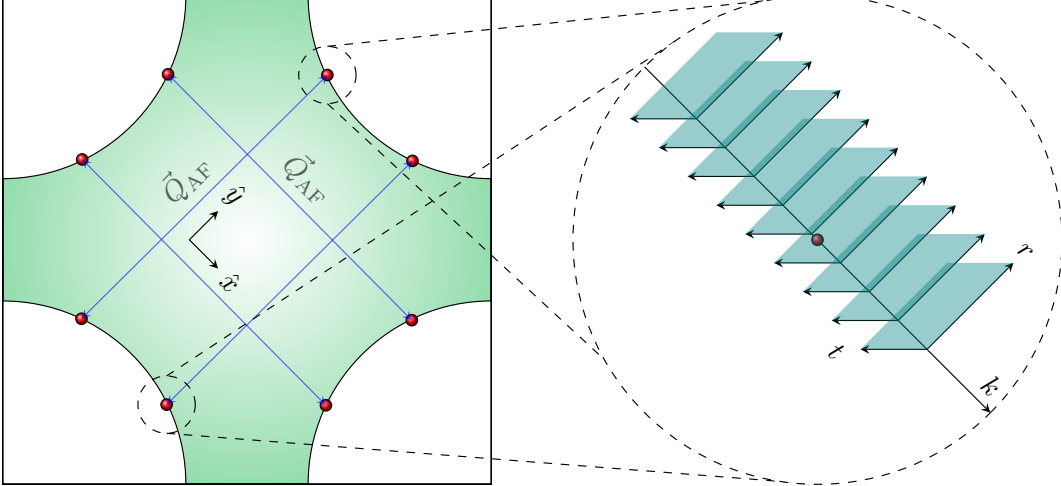


FIG. 4: The spinor composed of the electrons in segments 1 and 5 is defined in the hybrid spacetime  $(t, r, k)$ , where  $t$  is time,  $r$  is space conjugate to  $k_y$  and  $k = k_x$ .

the Fermi surface except at the hot spots. The dynamics of the fully renormalized quasiparticles is described by the quadratic action<sup>5</sup> in Eq. (12) with

$$v_k = \begin{cases} v_0(\ell_k^{(2L)}) & 0 \leq k < k_c \\ v_0(0) & k_c \leq k \end{cases} \quad \text{and} \quad \mathcal{V}_{F,k} = \begin{cases} \mathcal{E}_1(\ell_k^{(2L)}, 0)^{-1} & 0 \leq k < k_c \\ 1 & k_c \leq k \end{cases}. \quad (13)$$

As expected,  $\mathcal{V}_{F,k} = 1$  for  $k > k_c$  and vanishes at the hot spots.

There are two noteworthy features in Eq. (13). First, in  $k^* < k < k_c$ ,  $\mathcal{V}_{F,k}$  can be approximated to

$$\mathcal{V}_{F,k} = \left( \frac{k}{k_c} \right)^{\alpha_1} \quad \text{with} \quad \alpha_1 = \frac{\sqrt{N_c - 1}}{\sqrt{\ell_0} \log \ell_0}. \quad (14)$$

In this range of momentum,  $\mathcal{V}_{F,k}$  scales with  $k$  algebraically while  $v_k$  depends on  $k$  only logarithmically. This is because the quantum correction that renormalizes  $\mathcal{V}_{F,k}$  is stronger than what renormalizes  $v_k$ [14]. As a result,  $v_k$  is almost momentum-independent except in the vicinity of the hot spot within  $k < k^*$ ,

$$v_k \approx \begin{cases} v_0(\ell_k^{(2L)}) & 0 \leq k \leq k^* \\ v_0(0) & k^* < k \end{cases}, \quad (15)$$

where  $k^* = \frac{\Lambda e^{-\ell_0}}{4v_0(0)}$  is the momentum scale below which the flow of the nesting angle is appreciable<sup>6</sup>. Second, if one ignores the  $k$ -dependence of  $v_k$  in  $k > k^*$ , both  $x$  and  $y$  components of Fermi velocity are renormalized in the same fashion although there is no symmetry that protects the direction of the Fermi velocity. This peculiarity arises because the dominant renormalization of Fermi velocity is from the quantum correction to the frequency-dependent ( $ik_0$ ) term of the action in Eq. (1)[14]. In other words, the momentum dependence of  $\mathcal{V}_{F,k}$  arises because the strength of the quantum correction that dilates frequency depends on momentum along the Fermi surface. In the scheme that uses one global clock for the entire system, we are forced to transfer the momentum dependence of the quantum correction to the field renormalization and Fermi velocity. While this is a perfectly legitimate picture, what the theory is really suggesting is to view the momentum-dependent Fermi velocity as a non-uniform temporal metric on the Fermi surface. Here, we adopt this perspective in which electrons have momentum-independent Fermi velocity in  $k^* < k < k_c$  once the velocity is measured with a proper time defined with respect to a momentum-dependent metric.

<sup>5</sup> Besides the quadratic action, there also exists the four-fermion coupling that has been generated by the critical spin fluctuations. However, their effects on the quasiparticle motion is sub-leading compared to the quantum corrections that have been already incorporated into  $v_k$  and  $\mathcal{V}_{F,k}$  in the limit that the nesting angle is small.

<sup>6</sup>  $k^*$  is determined from  $\ell_0 = \ell_{k^*}^{(2L)}$ . Because the nesting angle flows slowly with  $\frac{v_{k_c}}{v_0} \approx 1 + \frac{\ell_{k_c}^{(2L)}}{\ell_0}$  for  $\ell_k^{(2L)} \ll \ell_0$ , we can use  $v_k \approx v_0(0)$  for  $k > k^*$ .

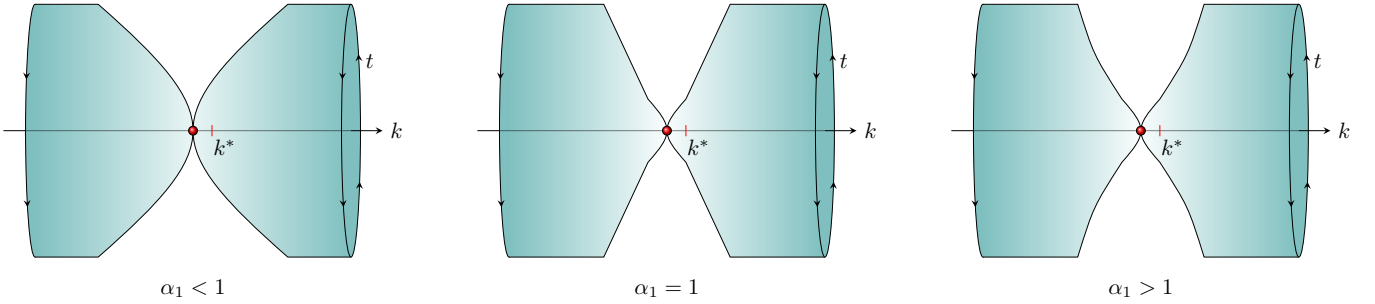


**FIG. 5:** The two-dimensional slice of the hybrid spacetime with a fixed  $r$ , where the imaginary time has been compactified with periodicity  $\beta$  for the purpose of visualization. In  $k \gg k_c$ , the proper length of the temporal circle remains  $\beta$ . In  $k^* < k < k_c$ , the proper length scales with  $k$  algebraically with exponent  $\alpha_1$ . In  $k < k^*$ , the power-law decay is replaced with a slower decay due to a flow of the nesting angle.

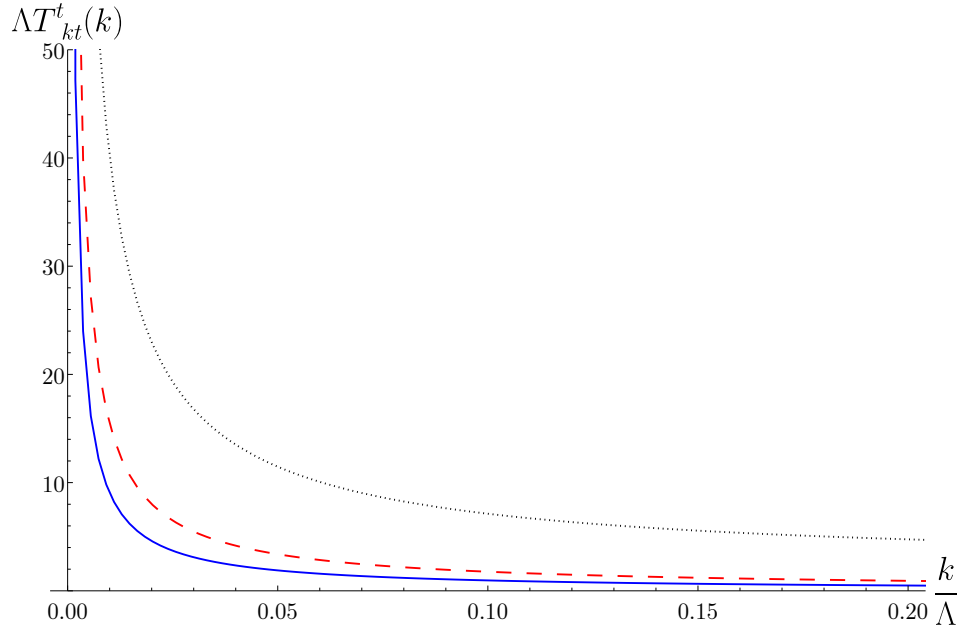


**FIG. 6:** The non-zero component of torsion shown as a function of momentum along the Fermi surface near the hot spots. The solid blue, dashed red and dotted black curves correspond to  $v_0(0) \approx 0.04$ ,  $v_0(0) \approx 0.13$  and  $v_0(0) \approx 1.13$ , respectively.

We formulate this geometric description by casting Eq. (12) into a theory of quasiparticles propagating in a curved spacetime[53] that incorporates the momentum-dependent metric. For this, we view the Fermi surface as a collection of 1+1-dimensional Dirac fermions stacked along the direction of Fermi surface, and combine a pair of chiral fermions at anti-podal points of the Fermi surface into a two-component Dirac spinor[54]. In this representation, Eq. (12) for segments 1 and 5 can be written as

$$S_{\text{kin}} = \sum_{\sigma=1}^{N_c} \sum_{j=1}^{N_f} \int \frac{dk}{2\pi} \int dt dr |\epsilon| \bar{\Psi}_{\sigma,j}(t, r, k) \{ \gamma^0 \epsilon_0^t D_t + \gamma^1 \epsilon_1^r D_r \} \Psi_{\sigma,j}(t, r, k). \quad (16)$$

Here, the hot spot index is dropped as we focus on  $N = 1$  and 5<sup>7</sup>. The theory is written in the hybrid spacetime of  $(t, r, k)$ [52], where  $t$  is time,  $r$  is the conjugate variable of  $k_y$ , and  $k = k_x$  labels points on the Fermi surface in segments 1 and 5 (See Fig. 4).  $\Psi_{\sigma,j}(t, r, k_x) \equiv \int \frac{dk_0 dk_y}{(2\pi)^2} e^{i(\omega t + k_y r)} \begin{bmatrix} \psi_{1,\sigma,j}(\omega, k_x, k_y) \\ \psi_{5,\sigma,j}^*(-\omega, -k_x, -k_y) \end{bmatrix}$  denotes the two-component

<sup>7</sup> It is straightforward to write down the theory for other segments.

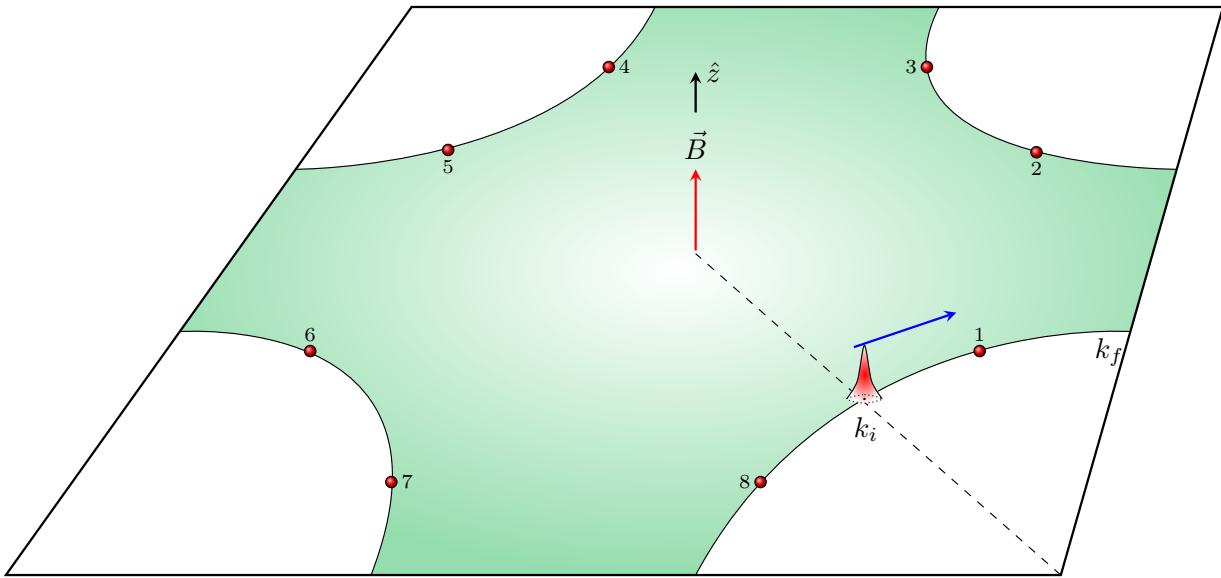


**FIG. 7:** The initial wavepacket of a quasiparticle is placed at the boundary between segments 1 and 8 ( $k_i$ ). In the presence of magnetic field applied in the  $z$  direction, the wavepacket moves along the Fermi surface. As it approaches hot spot 1, it slows down due to the momentum-dependent red shift.

spinor made of the quasiparticle fields in segments 1 and 5 and  $\bar{\Psi} = \Psi^\dagger \gamma^0$ , where  $\gamma^0 = \sigma_y$ ,  $\gamma^1 = \sigma_x$ ,  $\gamma^2 = \sigma_z$  denote  $2 \times 2$  gamma matrices that furnish the two-dimensional spinor representation.  $\epsilon_a^\mu$  is the inverse of the vielbein  $\epsilon_a^\mu$  with  $a = 0, 1, 2$  and  $\mu = t, r, k$ . The vielbein determines the metric in the  $2 + 1$ -dimensional spacetime through  $g_{\mu\nu} = \sum_{a=0}^2 \epsilon_a^\mu \epsilon_a^\nu$ . In general, the vielbein is a function of  $t, r, k$ , but in our case it depends only on  $k$ :  $\epsilon^0_t(k) = \mathcal{V}_{F,k}$ ,  $\epsilon^1_r(k) = \epsilon^2_k(k) = 1$  with all other elements being zero. The  $t$ - $k$  slice of the momentum-spacetime is illustrated in Fig. 5.  $|\epsilon|$  is the determinant of  $\epsilon_a^\mu$ .  $D_\mu = \partial_\mu + \frac{i}{2} \omega_{\mu,ab} \Sigma^{ab} + i A_\mu$  denotes the covariant derivative, where  $\omega_{\mu,ab}$  is the spin connection with  $\Sigma^{ab} = \frac{i}{4} [\gamma^a, \gamma^b]$  and  $A_\mu$  is the U(1) gauge field. Eq. (16) becomes equivalent to Eq. (12) for the trivial spin connection  $\omega_{\mu,ab} = 0$  and the gauge field given by  $A_t = 0$ ,  $A_r = v_k k$ ,  $A_k = 0$ . The gauge field  $A_r$  gives a  $k_x$ -dependent shift of momentum in the  $r$  direction so that quasiparticles have zero energy at  $k_y = -v_{k_x} k_x$ . With the vielbein and spin connection fully fixed by the renormalized coupling functions, Cartan's structure equation determines the torsion of the spacetime to be  $T^t = \frac{1}{\mathcal{V}_{F,k}} \frac{d\mathcal{V}_{F,k}}{dk} dk \wedge dt$ ,  $T^r = T^k = 0$ . The non-zero component of the torsion diverges in the  $k \rightarrow 0$  limit as is shown in Fig. 6.

Eq. (16) describes quasiparticles moving in a curved hybrid spacetime with a non-trivial torsion. It expresses the fact that the Fermi velocity along the direction of  $\vec{Q}_{AF}$  is 1 everywhere on the Fermi surface if the momentum-dependent proper time interval  $d\tau = \epsilon^0_t(k) dt$  is used in measuring velocity at momentum  $k$ . The ‘apparent’ variation of Fermi velocity arises only when one chooses to probe the dynamics of quasiparticles in one fixed clock. For an external lab observer whose clock ticks once for every unit proper time defined in  $k > k_c$ , quasiparticles appear to slow down near hot spots due to the momentum-dependent red-shift in the same way that a free falling object appears to undergo a slower time evolution near the surface of a massive object with respect to the far observer due to the gravitational red shift.

### III. Cyclotron motion of quasiparticles in the curved momentum-spacetime

In this section, we examine how the curved momentum-spacetime affects the dynamics of quasiparticles by computing the cyclotron period of electron in the presence of magnetic field<sup>55, 56</sup>. Due to the  $C_4$  and reflection symmetry, the cyclotron period at bare nesting angle  $v_0$ <sup>8</sup> can be written as  $T(v_0) = 8 [T(k_i, 0; v_0) + T(0, k_f; v_0)]$ , where  $T(k_i, 0; v_0)$  denotes the time that it takes for a quasiparticle to traverse from the boundary between segments 1 and 8 to hot spot 1, and  $T(0, k_f; v_0)$ , from hot spot 1 to the Brillouin zone boundary between segments 1 and 6 (see Fig. 1). The setup

<sup>8</sup> In this section, we use  $v_0$  and  $v_0(0)$  interchangeably for the momentum-independent bare nesting angle.

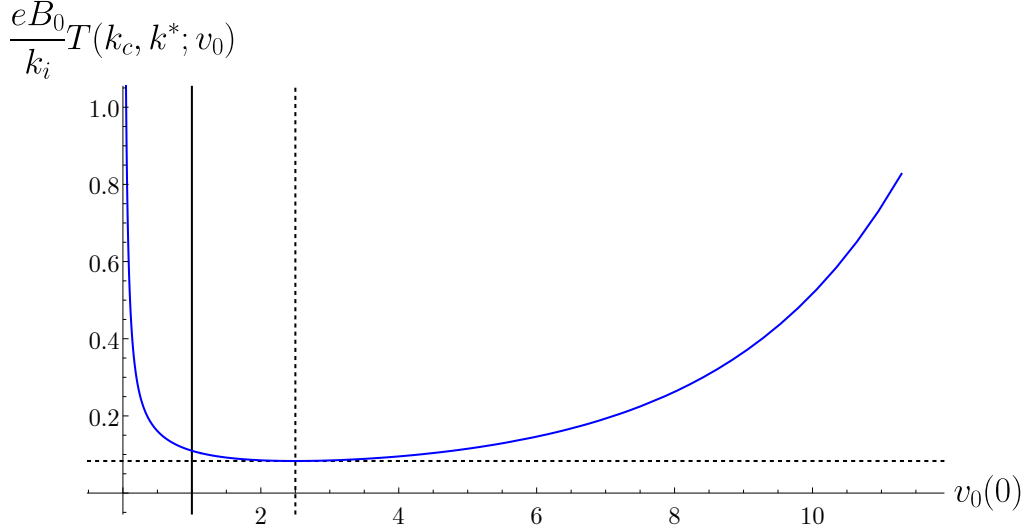


**FIG. 8:** The time that it takes for a quasiparticle to traverse from  $k_c$  to  $k^*$  plotted in the unit of  $k_i/(eB_0)$  as a function of the bare nesting angle for  $k_i/\Lambda = 6$ . The solid vertical line denotes the nesting angle at which  $\alpha_1 = 1$ . The dashed lines mark the minimum of  $T(k_c, k_i; v_0)$ .

is depicted in Fig. 7. For simplicity, we assume  $T(0, k_f; v_0) = T(k_i, 0; v_0)$  and focus on the computation of  $T(k_i, 0; v_0)$  here<sup>9</sup>.

In the zero temperature limit, there exist well-defined quasiparticles away from the hot spots and we can use the semi-classical description for their dynamics. The equation of motion for the position and momentum of the wavepacket of a quasiparticle reads

$$\frac{1}{\epsilon_t^0} \frac{d\vec{r}}{dt} = \left( k \frac{\partial v_k}{\partial k} + v_k \right) \hat{x} + \hat{y}, \quad \frac{1}{\epsilon_t^0} \frac{d\vec{k}}{dt} = -eB_0 \left[ \hat{x} - \left( k \frac{\partial v_k}{\partial k} + v_k \right) \hat{y} \right], \quad (17)$$

where  $B_0$  is the magnetic field applied along the  $\hat{z}$  direction. Eq. (17) is obtained by replacing  $dt$  with the proper time interval  $d\tau = \epsilon_t^0(k)dt$  in the equation of motion for a quasiparticle with Fermi velocity  $(k dv_k/dk + v_k, 1)$ . This follows from the facts that the equation of motion of the wavepacket is local in  $\vec{k}$  as well as in  $\vec{r}$  and that the evolution of quasiparticle should depend only on the proper time. Alternatively, Eq. (17) can be derived from Eq. (11) as the standard equation of motion,  $\frac{d\vec{r}}{dt} = \mathcal{V}_{F,k} \left[ \left( k \frac{\partial v_k}{\partial k} + v_k \right) \hat{x} + \hat{y} \right]$ ,  $\frac{d\vec{k}}{dt} = -eB_0 \mathcal{V}_{F,k} \left[ \hat{x} - \left( k \frac{\partial v_k}{\partial k} + v_k \right) \hat{y} \right]$ , which describes a quasiparticle propagating in the flat momentum-spacetime but with Fermi velocity  $\mathcal{V}_{F,k}(k dv_k/dk + v_k, 1)$ .  $B_0$  is assumed to be weak so that it does not affect the renormalized coupling functions. We consider quasiparticles on the Fermi surface, which allows us to focus on the equation of motion for the momentum along the Fermi surface.

For  $k_c < k_i$ <sup>10</sup>, there exists a region of Fermi surface near the zone boundary where the renormalization from spin fluctuations is negligible at energies below UV cutoff  $\Lambda$ . In this case,  $T(k_i, 0; v_0)$  can be written as the sum of three intervals,  $T(k_i, 0; v_0) = T(k_i, k_c; v_0) + T(k_c, k^*; v_0) + T(k^*, 0; v_0)$ .  $T(k_i, k_c; v_0)$  denotes the time that the quasiparticle spends in the region where the quantum correction from spin fluctuations is negligible and the hybrid spacetime is almost flat.  $T(k_c, k^*; v_0)$  arises from the region with algebraically decaying  $\epsilon_t^0(k)$ . Finally,  $T(k^*, 0; v_0)$  denotes the time that the quasiparticle spends in the very vicinity of the hot spot where the flow of the nesting angle modifies the spacetime geometry from the algebraic form. In the following, we compute each time interval one by one.

In the cold region with  $k_c < k < k_i$ ,  $\epsilon_t^0 \approx 1$ . From  $\frac{d\vec{r}}{dt} = v_0(0)\hat{x} + \hat{y}$ ,  $\frac{d\vec{k}}{dt} = -eB_0(\hat{x} - v_0(0)\hat{y})$ , one readily obtains

$$T(k_i, k_c; v_0) = \frac{k_i - k_c}{eB_0}. \quad (18)$$

In  $k^* < k < k_c$ , the nesting angle can be still regarded as momentum-independent while the vielbein decays as

<sup>9</sup> In general,  $T(0, k_f; v_0) \neq T(k_i, 0; v_0)$ , but the computation of  $T(0, k_f; v_0)$  is exactly parallel to that of  $T(k_i, 0; v_0)$ .

<sup>10</sup> For this to be the case, we need  $k_i > \Lambda/(4v_0)$ .

$\epsilon_t^0 = (k/k_c)^{\alpha_1}$ , where the exponent  $\alpha_1$  is determined from the bare nesting angle through Eqs. (10) and (14). The equations of motion become

$$\frac{d\vec{r}}{dt} = \left(\frac{k(t)}{k_c}\right)^{\alpha_1} (v_0(0)\hat{x} + \hat{y}), \quad \frac{d\vec{k}}{dt} = -eB_0 \left(\frac{k(t)}{k_c}\right)^{\alpha_1} (\hat{x} - v_0(0)\hat{y}), \quad (19)$$

where  $k(t)$  denotes the  $x$ -component of  $\vec{k}(t)$ . Integrating  $\frac{dk(t)}{dt} = -eB_0 \left(\frac{k(t)}{k_c}\right)^{\alpha_1}$  from  $k_c$  to  $k^*$ , we obtain

$$T(k_c, k^*; v_0) = \frac{k_c^{\alpha_1}}{eB_0} \int_{k^*}^{k_c} \frac{dk'}{k'^{\alpha_1}} = \frac{k_c}{(1-\alpha_1)eB_0} \left[ 1 - \left(\frac{k^*}{k_c}\right)^{1-\alpha_1} \right]. \quad (20)$$

$T(k_c, k^*; v_0)$  is plotted as a function of  $v_0(0)$  in Fig. 8. For small nesting angle,  $T(k_c, k^*; v_0)$  rapidly decreases with increasing  $v_0(0)$ . This is because the range of lukewarm region decreases with increasing nesting angle for a fixed  $\Lambda$  (see Fig. 3). Furthermore, at larger nesting angles, even those electrons in the lukewarm region decouple from spin fluctuations at higher energy scales. Remarkably,  $T(k_c, k^*; v_0)$  bounces back as  $v_0(0)$  increases further. This non-monotonic behaviour is due to a competing effect that an increasing nesting angle has. At larger nesting angles, a reduction in the density of states of low-energy particle-hole excitations weakens the screening of interaction[18]. This makes the quantum-correction-induced red shift stronger for electrons close to the hot spots.

As the nesting angle increases, the portion of Fermi surface affected by spin fluctuations shrinks while electrons close to the hot spots are more significantly renormalized. The disparity in the strength of quantum correction in different parts of Fermi surface causes a more strongly curved spacetime at a large nesting angle. This is also reflected in the torsion that increases with increasing nesting angle as is shown in Fig. 6. The metric that becomes more singular at the hot spots with increasing nesting angle creates a possibility of realizing an analogous black hole horizon in momentum space. As  $\alpha_1$  approaches 1, the prefactor  $\frac{k_c}{(1-\alpha_1)eB_0}$  in Eq. (20) diverges and  $T(k_c, k^*; v_0)$  becomes

$$\lim_{\alpha_1 \rightarrow 1} T(k_c, k^*; v_0) = \frac{k_c}{eB_0} \log\left(\frac{k_c}{k^*}\right). \quad (21)$$

The leading small-angle expansion predicts that  $\alpha_1$  becomes 1 at  $v_0 \approx 1.13$  for  $N_c = 2$  and  $N_f = 1$ . Even though the small  $v_0$  expansion is not valid for theories with  $v_0 \sim 1$ , here we proceed with the assumption that the qualitative feature of the theory remains unchanged even at nesting angles that are not so small[40]. In this case, there may well be a critical nesting angle at which  $\alpha_1$  becomes 1 even if the actual critical value of  $v_0$  differs from what is predicted from the small- $v_0$  expansion. The way the time interval depends on  $k^*$  in Eq. (21) is reminiscent of the logarithmic divergence in the time needed for a free-falling object to reach the horizon of the Schwarzschild black hole as measured by an asymptotic observer. This is not a coincidence. It is a consequence of the fact that at  $\alpha_1 = 1$  the metric of a  $t$  and  $k$  slice of the hybrid spacetime in  $k > k^*$  is conformally equivalent to that of the Schwarzschild black hole outside the horizon. If  $k^*$  was zero, the cyclotron period would diverge and a quasiparticle would not be able to go through the hot spot for  $\alpha_1 \geq 1$ . In our case, the divergence is cut off by  $k^*$  because the momentum-spacetime geometry is modified from that of the Schwarzschild horizon for  $k < k^*$  due to the flow of the nesting angle<sup>11</sup>.

For  $0 < k < k^*$ , the electrons stay coupled with spin fluctuations at energy scales that are low enough that one has to consider the flow of the nesting angle. This modifies the temporal vielbein from the algebraic form to a ‘super-logarithmic’ form<sup>12</sup>,  $\epsilon_t^0 \approx \frac{1}{\nu(\ell_0)} \exp\left(-\sqrt{N_c^2 - 1} \frac{\sqrt{\ell_k^{(2L)} + \ell_0}}{\log \sqrt{\ell_k^{(2L)} + \ell_0}}\right)$ , where  $\nu(\ell_0) = \exp\left\{-\sqrt{N_c^2 - 1} \text{Ei}(\log \sqrt{\ell_0})\right\}$ . Because the nesting angle decreases in the vicinity of the hot spot, the quantum correction becomes weaker. As  $k$  approaches 0,  $\epsilon_t^0$  decreases to zero only as  $e^{-\sqrt{\log 1/k}}$ , which is slower than any power-law. This results in the time interval that remains finite even for  $\alpha_1 \geq 1$ ,  $T(k^*, 0; v_0) = \frac{\nu(\ell_0)}{eB_0} \int_0^{k^*} \exp\left(\sqrt{N_c^2 - 1} \frac{\sqrt{\ell_{k'}^{(2L)} + \ell_0}}{\log \sqrt{\ell_{k'}^{(2L)} + \ell_0}}\right) dk'$ . Substitution

$s = \sqrt{\ell_{k'}^{(2L)} + \ell_0}$  yields

$$T(k^*, 0; v_0) = \frac{\Lambda}{2v_0(0)} \frac{\nu(\ell_0)e^{\ell_0}}{eB_0} \int_{\sqrt{2\ell_0}}^{\infty} s \exp\left(-s^2 + \sqrt{N_c^2 - 1} \frac{s}{\log s}\right) ds. \quad (22)$$

<sup>11</sup> For this reason, the geometry that emerges in the  $\alpha_1 = 1$  limit is more a fuzzball[57] or a firewall[58] than a horizon with no ‘drama’. The fact that the horizon is a special place is also seen from the fact that the torsion diverges at the hot spots (see Fig. 6). Another difference from the Schwarzschild horizon is that there is no interior of the black hole in our analogous horizon.

<sup>12</sup> For this, we use  $\text{Ei}(X) \approx \frac{e^X}{X}$  for  $X \gg 1$ .

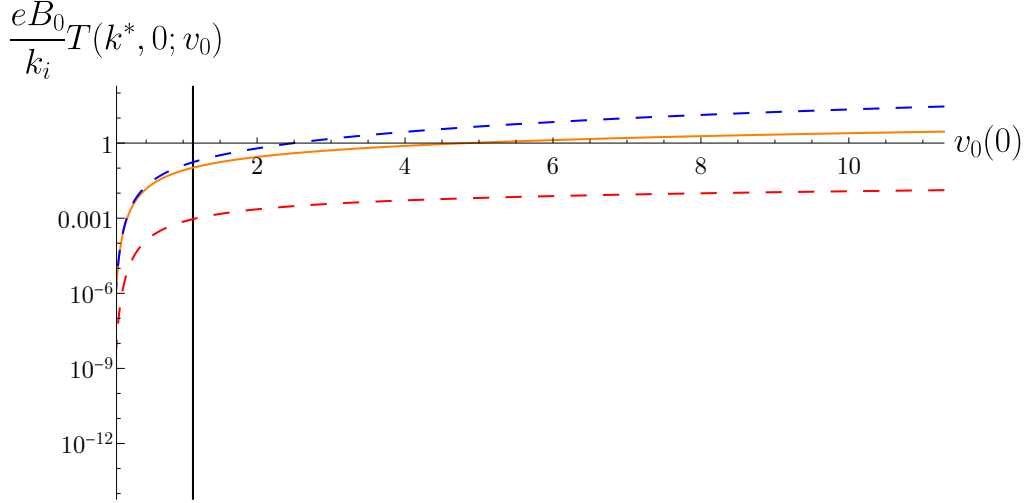


**FIG. 9:** The solid curve represents  $T(k^*, 0; v_0)$  plotted as a function of  $v_0(0)$ . Two dashed lines that sandwich the solid curve are upper and lower bounds whose expressions can be obtained analytically (see text). The vertical line marks the nesting angle at which  $\alpha_1 = 1$ .

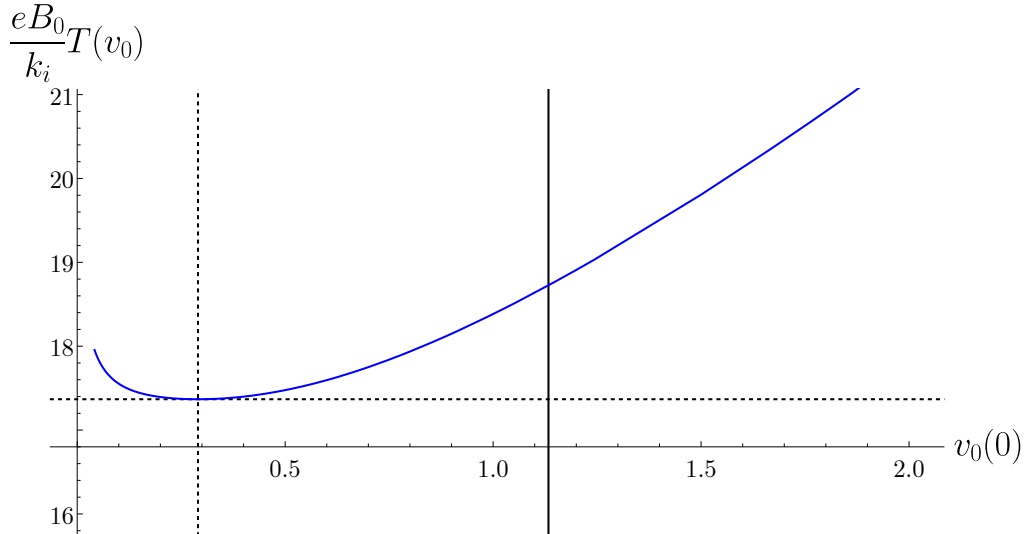


**FIG. 10:** The cyclotron period  $T(v_0)$  plotted as a function of the bare nesting angle for  $k_i/\Lambda = 6$ . The solid vertical line denotes the nesting angle with  $\alpha_1 = 1$ , and the dashed lines mark the minimum of  $T(v_0)$ .

It is hard to evaluate Eq. (22) exactly. But, we can bound it as  $T^{(l)}(k^*, 0; v_0) < T(k^*, 0; v_0) < T^{(u)}(k^*, 0; v_0)$ , where the lower bound is obtained by dropping  $s/\log s$  in the exponent on the integrand of Eq. (22),  $T^{(l)}(k^*, 0; v_0) = \frac{\nu(\ell_0)}{eB_0} k^*$ , and the upper bound is obtained by using  $\log s \approx \log \sqrt{2\ell_0}$ ,

$$T^{(u)}(k^*, 0; v_0) = \frac{\nu(\ell_0)}{eB_0} k^* \left[ e^{\sqrt{N_c^2 - 1} \frac{\sqrt{2\ell_0}}{\log \sqrt{2\ell_0}}} + \sqrt{\frac{\pi(N_c^2 - 1)}{4}} e^{\frac{N_c^2 - 1}{4 \log^2 \sqrt{2\ell_0}} + 2\ell_0} \frac{1 + \operatorname{erf} \left( \frac{\sqrt{N_c^2 - 1}}{2 \log \sqrt{2\ell_0}} - \sqrt{2\ell_0} \right)}{\log \sqrt{2\ell_0}} \right]. \quad (23)$$

Here,  $\operatorname{erf}(z) = \frac{2}{\sqrt{\pi}} \int_0^z e^{-t^2} dt$  is the error function. Fig. 9 shows  $T(k^*, 0; v_0)$ ,  $T^{(u)}(k^*, 0; v_0)$  and  $T^{(l)}(k^*, 0; v_0)$  as functions of  $v_0(0)$ . This shows that  $T(k^*, 0; v_0)$  is finite even for  $v_0$  with  $\alpha_1 \geq 1$ . The cyclotron period given by  $T(v_0) = 16 [T(k_i, k_c; v_0) + T(k_c, k^*; v_0) + T(k^*, 0; v_0)]$  is plotted in Fig. 10. The non-monotonic behaviour of  $T(v_0)$  as a function of  $v_0$  is the result of the increasing disparity in the strength of red shift across the Fermi surface with increasing  $v_0$ .

So far, we have consider the zero-temperature limit in which the entire Fermi surface supports coherent quasiparticles except at the hot spots. In reality, the superconducting instability is inevitable in theories with non-zero bare nesting angle[14], and we have to consider a non-zero temperature to be in the normal state. At temperature  $\mathcal{T}$  that is higher than the energy scale below which the nesting angle flows ( $\mathcal{T} > \Lambda e^{-\ell_0}$ )<sup>13</sup>, the expression for the cyclotron period should be revised to  $T(v_0) = 16 [T(k_i, k_c; v_0) + T(k_c, k^\#; v_0) + T(k^\#, 0; v_0)]$ . Here  $T(k_i, k_c; v_0)$  in Eq. (18) is unchanged.  $T(k_c, k^\#; v_0)$  is still given by Eq. (20) except that  $k^\# \sim \mathcal{T}/v$  now represents the momentum cut-off scale associated with temperature  $\mathcal{T}$ . Finally,  $T(k^\#, 0; v_0)$  represents the time that it takes for an incoherent electron pass through the hot region. In the small  $v_0$  limit, the quasiparticle is only marginally destroyed and it can estimated to be  $T(k^\#, 0; v_0) \sim \frac{k^\#}{eB_0(k^\#/k_c)^{\alpha_1}}$ .

In the zero-temperature superconducting state[14], one has to include the effect of the pair condensate to describe the dynamics of the Bogoliubov quasiparticles. Suppose that the ground state has the d-wave pairing[59] with a momentum-dependent pairing wavefunction  $\Delta_k$ . For the physical case with  $N_c = 2$  and  $N_f = 1$ , we need to add the following action for quasiparticles in segments 1 and 5,

$$S'^{1,5} = \sum_{\sigma, \sigma'=\uparrow, \downarrow} \int \frac{d\omega d^2k}{(2\pi)^3} \left\{ \psi_{1,\sigma}^*(\omega, \vec{k}) \Delta_k^{\sigma\sigma'} \psi_{5,\sigma'}^*(-\omega, -\vec{k}) + \psi_{5,\sigma}(-\omega, -\vec{k}) \Delta_k^{\dagger \sigma\sigma'} \psi_{1,\sigma'}(\omega, \vec{k}) \right\}, \quad (24)$$

where  $\Delta_k^{\sigma\sigma'} = \Delta_k \epsilon^{\sigma\sigma'}$  with  $\epsilon = \begin{pmatrix} 0 & 1 \\ -1 & 0 \end{pmatrix}$ . Eqs. (12) and (24) can be combined into an action of a spinor field that represents Bogoliubov quasiparticles in the superconducting state,

$$S_{\text{kin}}^{1,5} + S'^{1,5} = \int \frac{d\omega d^2k}{(2\pi)^3} \Psi(\omega, \vec{k}) \{i\omega \Gamma^0 + i\mathcal{V}_{F,k}(v_k k_x + k_y) \Gamma^1 - i\Delta_k \Gamma^2\} \Psi(\omega, \vec{k}), \quad (25)$$

where  $\Psi^T(\omega, \vec{k}) = (\psi_{1,\uparrow}(\omega, \vec{k}), \psi_{1,\downarrow}(\omega, \vec{k}), \psi_{5,\downarrow}^*(-\omega, -\vec{k}), -\psi_{5,\uparrow}^*(-\omega, -\vec{k}))$  is a 4-component spinor.  $\Psi(\omega, \vec{k}) = \Psi^\dagger(\omega, \vec{k}) \Gamma^0$  with  $\Gamma^0 = \sigma_y \otimes \mathbb{1}_2$ ,  $\Gamma^1 = \sigma_x \otimes \mathbb{1}_2$ ,  $\Gamma^2 = \sigma_z \otimes \mathbb{1}_2$  being  $4 \times 4$  gamma matrices, where the first Pauli matrices act on the Nambu spinor basis and the second Pauli matrices act on the spin space. In the hybrid momentum-spacetime, Eq. (25) can be written as

$$S_{\text{kin}}^{1,5} + S'^{1,5} = \int \frac{dk}{2\pi} \int dt dr |\epsilon| \bar{\Psi}(t, r, k) \{\Gamma^0 \epsilon_0^t D_t + \Gamma^1 \epsilon_1^r D_r\} \Psi(t, r, k). \quad (26)$$

Here, the vielbein and the U(1) gauge field are unchanged, but the pairing term gives rise to a complex spin connection,  $\omega_{t,02} = 4i\Delta_k$ . It will be of interest to find geometric interpretation of physical observables in the superconducting state.

#### IV. Conclusion

In this paper, we show that the momentum-dependent quantum correction that dilates frequency of electron anisotropically on the Fermi surface gives rise to a curved momentum-spacetime for low-energy quasiparticles in the 2+1 dimensional antiferromagnetic quantum critical metal. The non-trivial dependence of the emergent geometry on the shape of the Fermi surface causes a non-monotonic dependence of the cyclotron frequency on the bare nesting angle of the Fermi surface. With increasing nesting angle, the stronger disparity in the strength of quantum correction in different parts of Fermi surface makes the momentum-dependent red shift more singular at the hot spots. This creates a possibility of realizing an analogous black hole horizon at the hot spots where the motion of quasiparticle tend to freeze beyond a critical bare nesting angle of the Fermi surface. However, this analogous horizon does not lead to a vanishing cyclotron frequency because the metric in the vicinity of the hot spots is modified by thermal effects above the superconducting transition temperature.

#### Acknowledgement

This research was supported by the Natural Sciences and Engineering Research Council of Canada. Research at the Perimeter Institute is supported in part by the Government of Canada through Industry Canada, and by the

<sup>13</sup> In the small  $v_0$  limit, the superconducting temperature is given by  $T_c \sim \Lambda e^{-\frac{a}{\sqrt{v_0 \log(1/v_0)}}}$  which is higher than the energy scale below which the nesting angle flows significantly,  $\Lambda e^{-\frac{b}{v_0 \log(1/v_0)}}$ , where  $a$  and  $b$  are constants independent of  $v_0$ [14].

Province of Ontario through the Ministry of Research and Information.

---

[1] D. Xiao, M.-C. Chang, and Q. Niu, *Reviews of Modern Physics* **82**, 1959 (2010).

[2] C. Crnkovic, *Classical and Quantum Gravity* **5**, 1557 (1988).

[3] J. Kowalski-Glikman, *International Journal of Modern Physics A* **28**, 1330014 (2013).

[4] J. Lee and R. M. Wald, *Journal of Mathematical Physics* **31**, 725 (1990), <https://doi.org/10.1063/1.528801>.

[5] A. Ashtekar, L. Bombelli, and O. Reula, in *Mechanics, Analysis and Geometry: 200 Years After Lagrange*, North-Holland Delta Series, edited by M. Francaviglia (Elsevier, Amsterdam, 1991) pp. 417–450.

[6] S. Davis and M. Foster, *SciPost Physics* **12**, 10.21468/scipostphys.12.6.204 (2022).

[7] B. Amorim, A. Cortijo, F. de Juan, A. Grushin, F. Guinea, A. Gutiérrez-Rubio, H. Ochoa, V. Parente, R. Roldán, P. San-Jose, J. Schiefele, M. Sturla, and M. Vozmediano, *Physics Reports* **617**, 1 (2016).

[8] Y. Wang, Z. Chi, and J. Liu, *Composite Structures* **258**, 113204 (2021).

[9] V. M. Pereira, A. C. Neto, H. Liang, and L. Mahadevan, *Physical review letters* **105**, 156603 (2010).

[10] J. Mao, S. P. Milovanović, M. Andelković, X. Lai, Y. Cao, K. Watanabe, T. Taniguchi, L. Covaci, F. M. Peeters, A. K. Geim, Y. Jiang, and E. Y. Andrei, *Nature* **584**, 215 (2020).

[11] M. Vozmediano, M. Katsnelson, and F. Guinea, *Physics Reports* **496**, 109 (2010).

[12] A. Cortijo and M. A. Vozmediano, *Nuclear Physics B* **763**, 293 (2007).

[13] T. B. Smith, L. Pullasser, and A. Srivastava, Momentum-space gravity from the quantum geometry and entropy of bloch electrons (2021), [arXiv:2108.02216 \[cond-mat.mes-hall\]](https://arxiv.org/abs/2108.02216).

[14] F. Borges, A. Borissov, A. Singh, A. Schlief, and S.-S. Lee, *Annals of Physics* **450**, 169221 (2023).

[15] T. Helm, M. V. Kartsovnik, I. Sheikin, M. Bartkowiak, F. Wolff-Fabris, N. Bittner, W. Biberacher, M. Lambacher, A. Erb, J. Wosnitza, and R. Gross, *Phys. Rev. Lett.* **105**, 247002 (2010).

[16] K. Hashimoto, K. Cho, T. Shibauchi, S. Kasahara, Y. Mizukami, R. Katsumata, Y. Tsuruhara, T. Terashima, H. Ikeda, M. A. Tanatar, H. Kitano, N. Salovich, R. W. Giannetta, P. Walmsley, A. Carrington, R. Prozorov, and Y. Matsuda, *Science* **336**, 1554 (2012).

[17] T. Park, F. Ronning, H. Yuan, M. Salamon, R. Movshovich, J. Sarrao, and J. Thompson, *Nature* **440**, 65 (2006).

[18] A. Schlief, P. Lunts, and S.-S. Lee, *Phys. Rev. X* **7**, 021010 (2017).

[19] A. Abanov and A. V. Chubukov, *Phys. Rev. Lett.* **84**, 5608 (2000).

[20] A. Abanov, A. V. Chubukov, and J. Schmalian, *Adv. Phys.* **52**, 119 (2003).

[21] A. Abanov and A. Chubukov, *Phys. Rev. Lett.* **93**, 255702 (2004).

[22] S. A. Hartnoll, D. M. Hofman, M. A. Metlitski, and S. Sachdev, *Phys. Rev. B* **84**, 125115 (2011).

[23] E. Abrahams and P. Wölfe, *Proc. Natl. Acad. Sci.* **109**, 3238 (2012).

[24] J. Lee, P. Strack, and S. Sachdev, *Phys. Rev. B* **87**, 045104 (2013).

[25] V. S. de Carvalho and H. Freire, *Nuclear Physics B* **875**, 738 (2013).

[26] A. A. Patel, P. Strack, and S. Sachdev, *Phys. Rev. B* **92**, 165105 (2015).

[27] C. M. Varma, *Phys. Rev. Lett.* **115**, 186405 (2015).

[28] S. A. Maier and P. Strack, *Phys. Rev. B* **93**, 165114 (2016).

[29] C. M. Varma, W. J. Gannon, M. C. Aronson, J. A. Rodriguez-Rivera, and Y. Qiu, *Phys. Rev. B* **97**, 085134 (2018).

[30] M. A. Metlitski and S. Sachdev, *Phys. Rev. B* **82**, 075128 (2010).

[31] S. Sur and S.-S. Lee, *Phys. Rev. B* **91**, 125136 (2015).

[32] S.-S. Lee, *Annu. Rev. of Condens. Matter Phys.* **9**, 227 (2018).

[33] E. Berg, M. Metlitski, and S. Sachdev, *Science* **338**, 1606 (2012).

[34] Z.-X. Li, F. Wang, H. Yao, and D.-H. Lee, *Science Bulletin* **61**, 925 (2016).

[35] Y. Schattner, M. H. Gerlach, S. Trebst, and E. Berg, *Phys. Rev. Lett.* **117**, 097002 (2016).

[36] M. H. Gerlach, Y. Schattner, E. Berg, and S. Trebst, *Phys. Rev. B* **95**, 035124 (2017).

[37] Z.-X. Li, F. Wang, H. Yao, and D.-H. Lee, *Phys. Rev. B* **95**, 214505 (2017).

[38] X. Wang, Y. Wang, Y. Schattner, E. Berg, and R. M. Fernandes, *Phys. Rev. Lett.* **120**, 247002 (2018).

[39] E. Berg, S. Lederer, Y. Schattner, and S. Trebst, Monte carlo studies of quantum critical metals (2018), [arXiv:1804.01988](https://arxiv.org/abs/1804.01988).

[40] P. Lunts, M. S. Albergo, and M. Lindsey, arXiv e-prints , arXiv:2204.14241 (2022), [arXiv:2204.14241 \[cond-mat.str-el\]](https://arxiv.org/abs/2204.14241).

[41] B. J. Ramshaw, S. E. Sebastian, R. D. McDonald, J. Day, B. S. Tan, Z. Zhu, J. B. Betts, R. Liang, D. A. Bonn, W. N. Hardy, and N. Harrison, *Science* **348**, 317 (2015).

[42] J. Custers, P. Gegenwart, H. Wilhelm, K. Neumaier, Y. Tokiwa, O. Trovarelli, C. Geibel, F. Steglich, C. Pépin, and P. Coleman, *Nature* **424**, 524 (2003).

[43] S. E. Sebastian, N. Harrison, E. Palm, T. P. Murphy, C. H. Mielke, R. Liang, D. A. Bonn, W. N. Hardy, and G. G. Lonzarich, *Nature* **454**, 200 (2008).

[44] S. E. Sebastian, N. Harrison, and G. G. Lonzarich, *Reports on Progress in Physics* **75**, 102501 (2012).

[45] A. Legros, K. W. Post, P. Chauhan, D. G. Rickel, X. He, X. Xu, X. Shi, I. Božović, S. A. Crooker, and N. P. Armitage, *Phys. Rev. B* **106**, 195110 (2022).

[46] S. K. Goh, P. L. Alireza, L. E. Klintberg, T. Murphy, F. Nakamura, D. J. Singh, and M. Sutherland, *Quantum oscillations in the high pressure metallic state of  $ca_2ruo_4$*  (2012), [arXiv:1205.3045 \[cond-mat.str-el\]](https://arxiv.org/abs/1205.3045).

- [47] N. Doiron-Leyraud, C. Proust, D. LeBoeuf, J. Levallois, J.-B. Bonnemaison, R. Liang, D. A. Bonn, W. N. Hardy, and L. Taillefer, *Nature* **447**, 565 (2007).
- [48] J. Singleton, C. de la Cruz, R. D. McDonald, S. Li, M. Altarawneh, P. Goddard, I. Franke, D. Rickel, C. H. Mielke, X. Yao, and P. Dai, *Physical Review Letters* **104**, 10.1103/physrevlett.104.086403 (2010).
- [49] S. Badoux, W. Tabis, F. Laliberté, G. Grissonnanche, B. Vignolle, D. Vignolles, J. Béard, D. Bonn, W. Hardy, R. Liang, et al., *Nature* **531**, 210 (2016).
- [50] V. Grinenko, K. Iida, F. Kurth, D. V. Efremov, S.-L. Drechsler, I. Cherniavskii, I. Morozov, J. Hänisch, T. Förster, C. Tarantini, J. Jaroszynski, B. Maiorov, M. Jaime, A. Yamamoto, I. Nakamura, R. Fujimoto, T. Hatano, H. Ikuta, and R. Hühne, *Scientific Reports* **7**, 10.1038/s41598-017-04724-3 (2017).
- [51] M. Kimata, T. Terashima, N. Kurita, H. Satsukawa, A. Harada, K. Kodama, K. Takehana, Y. Imanaka, T. Takamasu, K. Kihou, C.-H. Lee, H. Kito, H. Eisaki, A. Iyo, H. Fukazawa, Y. Kohori, H. Harima, and S. Uji, *Physical Review Letters* **107**, 10.1103/physrevlett.107.166402 (2011).
- [52] S. Sur and S.-S. Lee, *Phys. Rev. B* **90**, 045121 (2014).
- [53] N. D. Birrell and P. C. W. Davies, *Quantum Fields in Curved Space*, Cambridge Monographs on Mathematical Physics (Cambridge University Press, 1982).
- [54] D. Dalidovich and S.-S. Lee, *Phys. Rev. B* **88**, 245106 (2013).
- [55] T. D. Stănescu, V. Galitski, and H. D. Drew, *Physical Review Letters* **101**, 10.1103/physrevlett.101.066405 (2008).
- [56] T. Senthil, On the mass enhancement near optimal doping in high magnetic fields in the cuprates (2014), [arXiv:1410.2096 \[cond-mat.str-el\]](https://arxiv.org/abs/1410.2096).
- [57] S. D. Mathur, *Fortsch. Phys.* **53**, 793 (2005), [arXiv:hep-th/0502050](https://arxiv.org/abs/hep-th/0502050).
- [58] A. Almheiri, D. Marolf, J. Polchinski, and J. Sully, *Journal of High Energy Physics* **2013**, 62 (2013).
- [59] D. J. Scalapino, E. Loh, and J. E. Hirsch, *Phys. Rev. B* **34**, 8190 (1986).